Influence of overriding plate geometry and rheology on subduction

N. P. Butterworth and L. Quevedo

EarthByte Group, School of Geosciences, University of Sydney, Madsen Building, Sydney, New South Wales 2006, Australia (nathaniel.butterworth@sydney.edu.au; leonardo.quevedo@sydney.edu.au)

G. Morra

School of Earth and Environmental Sciences, Seoul National University, Gwanak–gu, Seoul 151–742, South Korea (gabrielemorra@gmail.com)

R. D. Müller

EarthByte Group, School of Geosciences, University of Sydney, Madsen Building, Sydney, New South Wales 2006, Australia (dietmar.muller@sydney.edu.au)

[1] Subduction dynamics is strongly dependent on the geometry and rheology of the subducting slab and adjacent plates, as well as on the induced mantle flow driven by the evolution of tectonic configurations along subduction zones. However, these processes, and the associated plate tectonic driving forces, are difficult to study using time-dependent 3-dimensional computer simulations due to limitations in computing resources. We investigate these phenomena with a novel numerical approach, using BEM-Earth, a Stokes flow solver based on the Boundary Element Method (BEM) with a Fast-Multipole (FM) implementation. The initial BEM-Earth model configurations self-consistently determine the evolution of the entire lithosphere-mantle system without imposing additional constraints in a whole-Earth spherical setting. We find that models without an overriding plate overestimate trench retreat by 65% in a 20 m.y. model run. Also, higher viscosity overriding plates are associated with higher velocity subducting slabs, analogue to faster oceanic plates subducting beneath more rigid continental lithosphere. In our models poloidal flows dominate the coupling between the down-going and overriding plates, with trench-orthogonal length variations in overriding plates inducing flows at least $\sim 2\times$ stronger than trench-parallel width variations. However, deformation in the overriding plate is related to its length and width, with narrower and longer plates extending more than wider and shorter plates.

1. Introduction

[2] Subduction of tectonic plates forms an integral aspect of mantle convection. However some aspects of the explicit forces driving this phenomenon remain ambiguous. Here we use a numerical model that helps elucidate the dynamics of subduction systems. The simplest numerical subduction models have down-going slabs that are driven purely by the negative buoyancy of the slab in a two dimensional domain with only a single subducting plate [e.g., *Ribe*, 2010; *Di Giuseppe et al.*, 2008], allowing for investigating the dynamics of the down-going slab. Extending this to three dimensions [*Morra et al.*, 2006; *Schellart et al.*, 2007; *Capitanio et al.*, 2009; *Morra et al.*, 2009; *Stegman et al.*, 2010a, 2010b; *Schellart et al.*, 2010] allows also investigation of the trench-parallel component of the subducting plate's effect on mantle dynamics. Recent studies have also considered the significant influence that the overriding plate, sometimes referred to as the upper plate, has on the down-going slab, both in a dynamic simulation environment [*Arcay et al.*, 2008; *Clark et al.*, 2008; *Yamato et al.*, 2009; *Capitanio et al.*, 2010; *van Dinther et al.*, 2010], and also from an observational perspective [*Lallemand et al.*, 2005; *Schellart*, 2008a]. Further, the relative contributions of the major plate driving forces are well resolved [*Conrad and Lithgow-Bertelloni*, 2004]. But still, the forces distributed between the subducting slab and the overriding plates through time have not yet been thoroughly investigated. As such we try to pin down the difference in overriding plate and subducting slab coupling forces arising from various tectonic configurations. A statistical analysis of the role of the overriding plate, the subducting plate, and correlations to mantle flow in controlling subduction is given by *Lallemand et al.* [2005].

[3] Here, we utilize a fast Stokes flow solver, BEM-Earth, to model lithospheric slab coupling processes with the mantle. The FM-BEM implementation in BEM-Earth is a novel numerical method that is well suited for plate tectonics modeling involving processes at planetary scales. Our BEM-Earth models depict free-subduction, where the down-going slabs are driven purely by the negative buoyancy of the slab. We analyze subduction zone geometries of varying overriding plate and subducting plate thickness, length, and width. The dynamic variations that result are inherited from the respective poloidal and toroidal mantle flows induced by the various geometrical set-ups. The rheology of the subducting plate and the surrounding environment (the mantle, near-by plates, etc) also have an influence on the

dynamics of the interacting plates. As such we also investigate various plate viscosity ratios between the overriding plate and subducting plate, and the affect these parameters have on the subduction dynamics. The overriding and subducting plates are coupled through mantle flow and interplate forces so there is an effect on the overriding lithosphere from the down-going slab, and conversely there is an effect that the overriding plate has on the subducting slab. *Becker and O'Connell* [2001] and *Becker and Faccenna* [2009] showed that velocity correlations were not very sensitive to edge forces, accordingly our models disregard intraplate interactions. Because of the computational efficiency of BEM-Earth, we are able to make use of a full three-dimensional spherical model for a number of consecutive model runs to explore the geometric and rheological parameters existing in natural subduction. Our numerical models reflect the 'mode 1' subduction style of laboratory models of *Bellahsen* [2005]. The style of subduction observed is also consistent with the 2D-BEM simulations of *Ribe* [2010] and the Finite Element simulations of *Di Giuseppe et al.* [2008] and *Capitanio et al.* [2010].

2. Boundary Element Method Model Setup

[4] We utilize BEM-Earth [*Morra et al.*, 2007], a BEM code with a FM implementation, that solves for Stokes flow over a given domain. The BEM [*Pozrikidis*, 1992] is a numerical method for solving linear partial differential equations formulated as boundary integral equations.

[5] BEM-Earth produces fully dynamic models, unconstrained by velocity boundary conditions, allowing for parameters of the system to be specified at input, including, viscosity, density, and geometry. Each iteration of the code then determines velocity and stress fields over each of the model's rheological isosurfaces. Each isosurface bounds a homogenous region characterized by an effective density and viscosity, representative as an average of their properties, in line with a well established modeling framework [*Capitanio et al.*, 2010; *Ribe*, 2010]. The viscosity contrast between each isosurface is fixed for the simulation, thus thermal effects are not considered in the model. Systematic simulations of different initial parameter choices are made, allowing for the determination of each parameter's influence on subduction within the model framework. A schematic cross-section of the model area of interest is shown in Figure 1 with the parameters explained in Table 1.
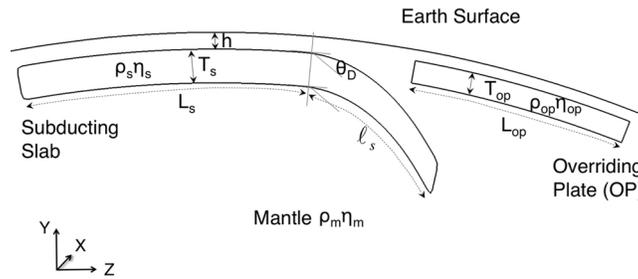
Figure 1. Diagram of a portion of the interacting plates model, with symbols defined. Mantle material permeates the intervening space between each isosurface. The separation of the isosurfaces is maintained by the contact parameters.

[6] Contact properties that influence the interactions between each model isosurface are initially defined. These parameters prevent the slab from detaching from the Earth surface and sinking vertically; rather the subducting plate advances in a more realistic fashion. There are several methods for providing a balancing buoyancy force in numerical models [*Morra et al.*, 2007; *Stegman et al.*, 2010a; *Ribe*, 2010] to keep the plate in local isostatic equilibrium. Here we use a 'lubrication layer' method, where the Earth boundary is described as an adaptive surface, whose dynamic behavior is controlled partially by the distance parameter h. The affect of the contact properties are analyzed in Appendix A and its method of operation is detailed in *Morra et al.* [2012, Appendix D].

[7] The density difference between the mantle and Earth surface self-consistently sustains the unsubducted lithosphere, as on the Earth, but lets the upper surface of the lithosphere free to deform in a full free-surface setting. The density difference drives the plates and the lubrication below the free-surface provides the normal stresses that prevent vertical sinking. During the simulation the Earth surface subsides under the weight of the lithosphere, generating an uplifting force [*Morra et al.*, 2007], reproducing the forcing controlling dynamic topography in the Earth.

[8] We use a spherical Earth made up of 20480 triangular elements on the surface, resulting in a resolution of about 29 km. By utilizing a spherical domain, we remove the consequences of pre-imposed artificial boundary conditions. A rectangular-prism plate is produced with an element resolution of about 24 km, and emplaced within the Earth. The Earth surface is then refined around where the plate is located. Additional isosurfaces are implemented (e.g., overriding plate, trailing plate, etc) as needed for each model. Mantle material permeates the Earth and the spaces between each isosurface. Spaces between isosurfaces vary as the models evolve, with a compressive regime imposed as the contact properties approach a minimum distance. There is no equivalent extensional algorithm at a distance, so the trench-ward pull on the overriding plate produced by suction is underestimated due to this gap.

[9] We maintain two reference models, one with a subducting plate only (Slab-Only), and one with an overriding plate (OP). Parameters used for model input are chosen based on well established parameters and other geodynamic models, detailed in Table 2. The geometric dimensions of the reference model are

Table 1. Model Symbol Definitions and Typical Initial Values

Parameter	Symbol	Value
Length of overriding plate	L_{op}	1274 km
Length of subducting plate	L_s	2038 km
Length of subducted portion of slab	ℓ_s	510 km
Dip angle	θ_D	45°
Thickness of slab	T_s	64 km
Thickness of overriding plate	T_{op}	64 km
Isosurface separation distance	h	26 km

Table 2. Reference Model Parameters

Parameter	Symbol	Value
Earth Radius	r_E	6371 km
Mantle Viscosity	η_m	10^{23} Pa · s
Mantle Density	ρ_m	3300 kg/m³
Slab Viscosity	η_s	50×10^{23} Pa · s
Slab Density	ρ_s	3400 kg/m³
Slab Width	W_s	2548 km
Slab Length	L_{sp}	2548 km
Slab Thickness	T_s	64 km
OP Viscosity	η_{op}	50×10^{23} Pa · s
OP Density	ρ_{op}	3270 kg/m³
OP Width	W_{op}	2548 km
OP Length	L_{op}	1274 km
OP Thickness	T_{op}	64 km

Table 3. Overriding Plate Model Dimensions

Model Name	OP Width (km)	OP Length (km)
Slab-Only	-	-
OP	2548	1274
OP-Wide	3822	1274
OP-Narrow	1274	1274
OP-Long	2548	2548
OP-Long/Wide	3822	2548
OP-Long/Narrow	1274	2548

chosen to reflect a small to medium Earth sized subducting plate. Rheology of the reference model is chosen as the most versatile (in terms of model stress testing) from a range of viscosities tried previously and based on other investigations [*Funiciello et al.*, 2003; *Schmeling et al.*, 2008; *Schellart*, 2008b; *Morra et al.*, 2012; *Capitanio et al.*, 2010; *van Dinther et al.*, 2010]. Versatile contact parameters are difficult to choose for a reference model, subducting plates may detach if they are not strong enough, and the plates may pierce the free Earth surface if they are too weak. Thus, we pick values empirically, that are stable for the greatest range of model parameter choices. Each model is run for 400 time steps, equivalent to about 25 m.y., the output velocity field data is then post-processed leading to the results in the succeeding sections.

[10] We do not consider subduction initiation, as we consider models that represent already established subduction zones which are self-sustaining and driven by the negative buoyancy of the slabs. 20% of the rectangular prism subducting plate is initially bent at a specified dip angle before being projected onto the free-surface sphere. This initial bending is to initiate subduction. The model then evolves freely under gravity through time.

[11] The mantle in the model is a homogeneous region with no rheological stratification. This causes slabs to approach vertical sinking with time, but otherwise, the dynamics under investigation are better isolated without the mantle heterogeneity observed in nature.

[12] Including a stiff core in preliminary models showed a negligible effect on the general dynamics of the plate interactions we consider in this paper. As such, the core was removed from the models for computational efficiency.

[13] In this analysis we do not model the ridge push force explicitly. However, ridge push can be considered by tapering the volume and density of the plate's trailing edge. We find that its impact on plate-mantle dynamics in our models is masked out by the surface contact layer. Since we determine this effect to be on average less than 1%, we use plates with constant thickness for simplicity.

3. Effects of the Overriding Plate on Subduction Dynamics
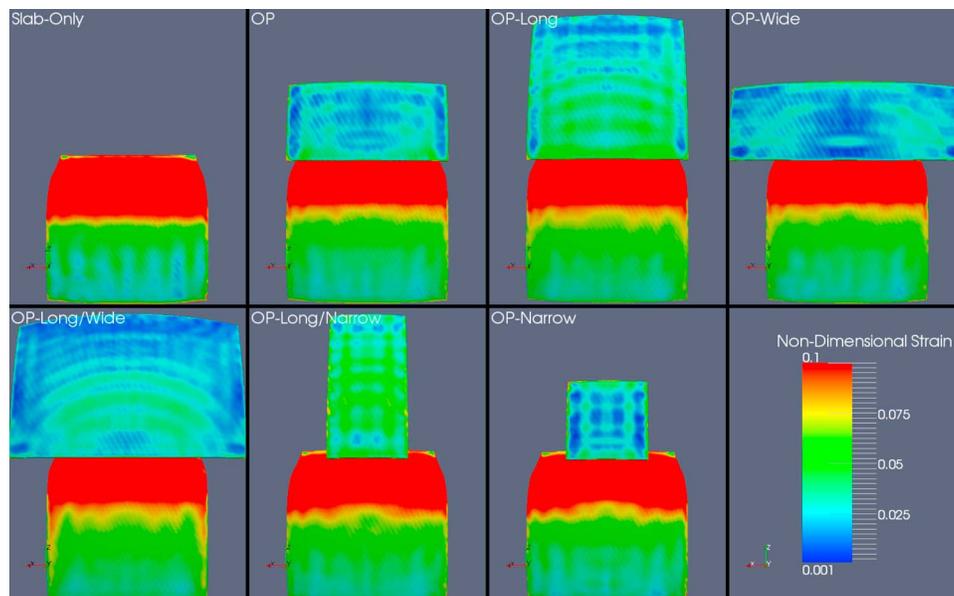
3.1. Dimensions of the Overriding Plate

[14] Geometrical dimensions of the overriding plate will influence the dynamics of the down-going slab. Here the rheological properties of the subducting plate are maintained, and the length and width of the overriding plate are systematically changed. The initial set-up for each model uses the reference parameters detailed in Table 2, but with different overriding plate dimensions, described in Table 3.

[15] We first consider the motion of the subduction trench as a way to contrast each model. The plot in Figure 2 shows the trench after 22 m.y. evolution. Trench location is defined as the point along the subducting plate corresponding to the minimum value of curvature, further explained in section 4. The Slab-Only model shows the trench rolling-back the furthest from the initial position, consistent with *Capitanio et al.* [2010]. All other models with overriding plates have rolled-back less substantially than the Slab-Only model. The OP-Wide model, behaves similarly to the OP model, indicating that overriding lithosphere extending laterally beyond the trench-parallel extent of the down-going slab has little affect on the subducting plate's evolution. The OP-Narrow model shows substantial slab-rollback on the edges of the subducting plate (where the overriding plate does not overhang) but shows similar trench migration to the OP model in the middle of the slab, further suggesting that the lateral spatial dimension of the overriding plate has a major affect on the down-going slab's evolution. As in the 2-D study of *Capitanio et al.* [2010], we find longer overriding plate models have similar trench shape development to the shorter models but with overall less evident rollback.

[16] The strain from the on-surface stress projection, seen at 10 m.y. in Figure 3, for the down-going plate in each model was found to remain similar regardless of the presence or shape of the overriding plate. Only deformation along the trench differs, along with timing of slab deformation, due to changed slab kinematics. However, the pattern of strain and the type of deformation in the overriding plate depends on its internal geometry. Generally, the strain distribution shows a circular intensity pattern radiating from trench side of the plate. The overall
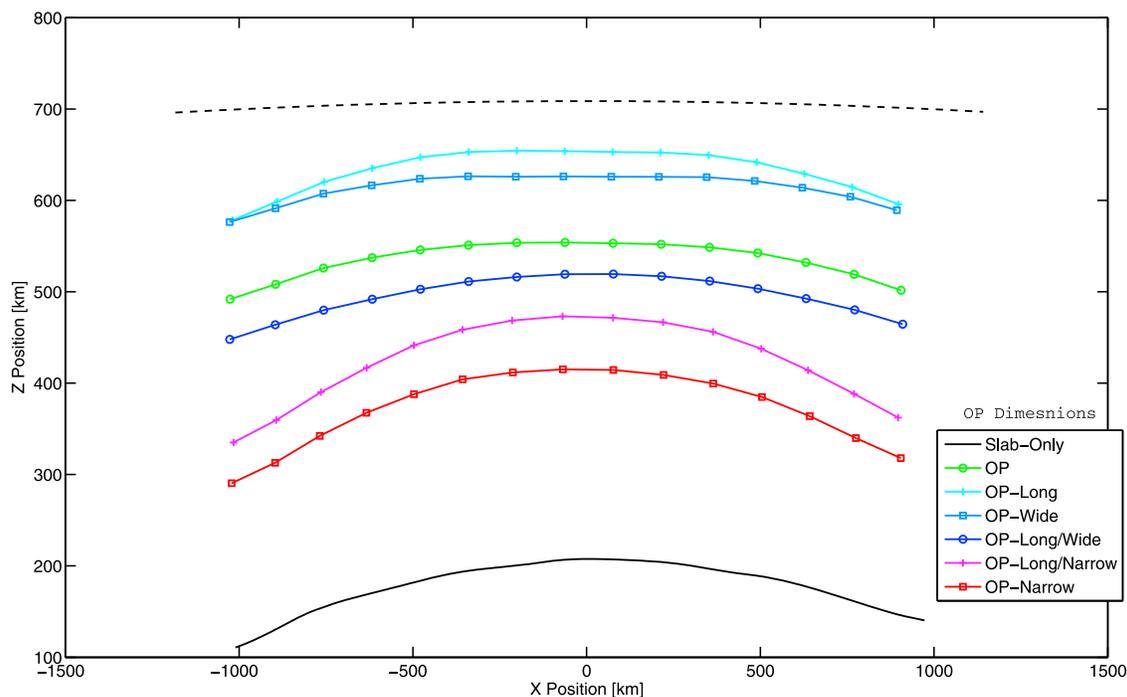
Figure 2. Trench morphology after 22 m.y. evolution projected onto the XZ-plane for the seven models with different size overriding plates. The dashed line shows the position at 0 m.y. for all models. The relative Z-position indicates amount of trench rollback.

Figure 3. Seven models each with different overriding plate dimensions. The models are labeled in the figure and the dimensions of each overriding plate are given in Table 3. The Earth free-surface has been removed to expose the plates. The colors represent strain after 10 m.y. model evolution, low strain indicates compression and high strain indicates extension. Viscosity in the down-going plate is the same as the overriding plate, leading to highly strained subducting plates.
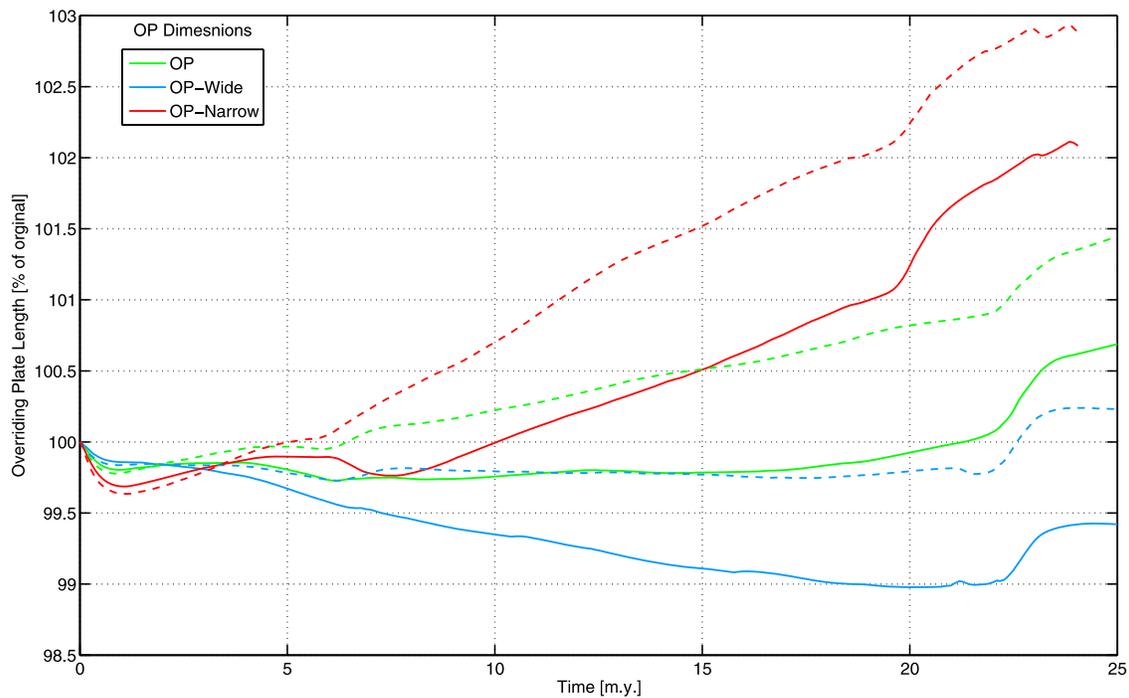
Figure 4. The length of the overriding plate through time for three models with different overriding plate widths. The solid lines are the deformation through the center of the overriding plate. The dashed lines represent a transect 500 km left of the center line.

trend of deformation can be seen in Figure 4, which shows the changing trench-orthogonal length of the overriding plate as the model evolves. In this figure, the three models immediately move into compression. At about 7 m.y. the OP-Narrow overriding plate begins to extend. The OP overriding plate is relatively undeformed until around 20 m.y. evolution when it begins extending rapidly. The OP-Wide overriding plate is continuously in a compressive regime, then around 22 m.y. there is a jump towards extension. After 20 m.y. the deformation of the three models along the center line are: OP-Narrow; 1.3%, OP; −0.1%, and OP-Wide; −1.0%, where positive deformation is extension. The same relative deformation regimes were found for longer over-riding plate models but with each overriding plate showing more extension (OP-Long/Narrow; 4.9%, OP-Long; 2.9%, and OP-Long/Wide; 2.0% after 20 m.y.) than the shorter models with equivalent widths. We note that the rate of deformation in our models is generally low compared with that observed in nature.

[17] Poloidal flows induced by the overriding plate only affect the region of subducting plate inline with the trench-parallel lateral extent of the overriding plate. In 2-D studies [e.g., *Ribe*, 2010], a slab descending

into the mantle produces a flow that goes down and under the slab, due to the displacement of the slab material entering the mantle. However in 3-D, material is displaced laterally around the edges as well, resulting in the subducting plate curving along the trench-parallel direction as highlighted in Figure 2. The two narrow models have steeply curved edges similar to the Slab-Only model. Whereas the other four models have similarly curved trenches.

3.2. Influence of Plate Width

[18] Subducting plate speed is found to scale with overriding plate geometric dimensions. The trench-orthogonal length of the overriding plate plays a role in scaling the speed of the subducting plate, with longer overriding plates having faster down-going slabs. The width of the overriding plate has a less substantial role in controlling subducting plate kinematics, but generally wider overriding plates have faster down-going slabs than models with narrower overriding plates. The Slab-Only model has the slowest subducting-plate of the models, moving around half the speed of (the fastest) OP-Long/Wide subducting plate. However, if the subducting plate width is scaled up with the overriding plate width, we find that the subducting plate speed increases with

width. This result is consistent with *Stegman et al.* [2006] and *Schellart et al.* [2010], who found subducting plate width scales with trench and subducting plate velocity in a 3-D cartesian box environment without an overriding plate.

[19] As the width increases the curvature of the subduction zone increases due to the faster velocities away from slab edges. With an overriding plate present the total degree of bending decreases. The general bending is suggested to be due to the curvature of the Earth and also the flow associated with each size plate [*Morra et al.*, 2009; *Mahadevan et al.*, 2010]. The width of the subducting plate will determine the concavity of the trench. A wide subducting plate will be convex, and a narrow subducting plate will be concave. The edges of the wide trenches were shown to have the same flexural shape as subduction zones presented in *Schellart et al.* [2007].

3.3. Influence of Overriding Plate Thickness

[20] Changing the thickness of the overriding plate has a minimal effect on subduction dynamics. This behavior in our three-dimensional free-subduction setting is comparable to the one obtained by *Capitanio et al.* [2010] in a two-dimensional setting. It is observed that thin overriding plates deform more than thicker plates, but the thickness does not influence the subducting slab.

3.4. Influence of a Trailing Plate

[21] A 2548 × 1274 × 64 km plate is introduced behind the subducting plate, referred to as the *trailing plate*. The internal properties are the same as the subducting plate. The length of the gap, L_{gap}, between the trailing plate and the back of the subducting plate is varied between 127–637 km. The trailing plate has the effect of slowing the advance of the subducting plate due to small scale convection in the intervening gap. The L_{gap} distance does not significantly change the coupling between the two plates as the slab dynamics are found to be consistent between each model.

[22] We also compare the trailing plate model with a model that replaces the subducting and trailing plates with one long plate of length $\ell + L_s + L_{gap} + L_{trailing}$. We confirm gap induced dynamics are not a consequence of the length of L_{gap}, but of the gap itself. The presence of any gap appears to change how much the subducting plate will advance as compared to rollingback. This result in our model is expectedly opposed to natural observations, where a ridge push force

would be actively pushing the advance of the subducting plate. Inclusion of the gap between the subducting plate and trailing plate causes the slab to advance and subduct more for equivalent time. The resulting dynamics of the down-going slab, in the presence of any trailing plate, bears analogy to the conclusions by *Funiciello et al.* [2004]; *Schellart* [2005]; *Stegman et al.* [2010b] of a trailing edge boundary condition having a dominant role in determining the morphology of the slab.

3.5. Influence of Lateral Plates

[23] Emplacing large non-subducting plates adjacent to the subducting plate changes the rate of subduction and the angle of dip. The subducting slab is slowed and the dip angle is decreased compared to a model without the surrounding plates. This same result was found by *Yamato et al.* [2009] in a 3-D cartesian box.

[24] The dynamics of a subducting slab are controlled by more than its internal negative buoyancy force. Adjacent non-subducting plates (overriding, lateral, and trailing plates) affect mantle flows. The non-subducting model isosurfaces act as a conduit to direct the mantle flows induced by the downgoing slab. This results in the subducting plate experiencing higher mantle drag and slab suction forces.

3.6. Viscosity of an Overriding Plate

[25] We analyze several models with different overriding plate viscosity values, to determine how ocean-ocean and ocean-continent subduction may differ, addressing the heterogeneity of plate rheology and the possibility that continental lithosphere is more viscous than the oceanic lithosphere [*Zhong*, 2001]. Each model's overriding plate viscosity is changed from $10–300 \times \eta_m$, whilst all other parameters take the values from Table 2. Models exhibit similar behavior in two distinct overriding plate viscosity regimes, high-viscosity or low-viscosity. The turning point between regimes for our model is found to be $\eta_{op} = 180 \times \eta_m$.

[26] Figure 5 shows a sample cross-section of the high-viscosity and low-viscosity models, along with Slab-Only model, after 15 m.y. evolution. We remark how the flow differs between the models, specifically from the altered shape of the slab. Low-viscosity overriding plate models have greater upturned slab tips than high-viscosity overriding plates. The slab tip in the low-viscosity overriding plate models approach the morphology of the Slab-
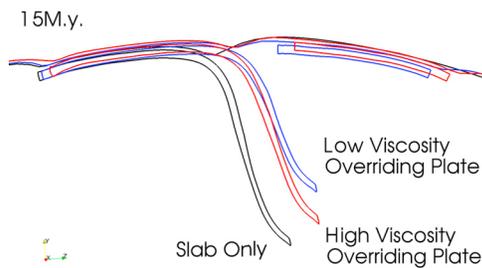
15 M.y.

Figure 5. Slice of models with different overriding plate viscosities at 15 m.y. High-viscosity model has $\eta_{op} = 300\eta_m$, the low-viscosity models has $\eta_{op} = 50\eta_m$, and the Slab-Only model is shown in black. Isostatic compensation in BEM-Earth causes the models to move relatively to each other, causing some of the offset between models, but absolute motions are still accurate.

Only model. The deep subduction in the Slab-Only model is allowed because there is no overriding plate to couple to. Because the total energy of the system is conserved, energy is dissipated by deforming the overriding plate more when the viscosity is low, so when there is a high-viscosity overriding plate, energy is available to drive the slab down faster. This in-turn drives the distance between the overriding plate and the trench, thereby increasing the distance for high-viscosity models and decreasing it (approaching the minimum allowed by the contact algorithm) for the low-viscosity models. Following from this, we find the dip of the slab at the trench is slightly steeper, at equivalent times, when a high-viscosity overriding plate is present. However, the angle of dip in all models will be steep due partially to the lack of mantle layering in our BEM-Earth model setup.

[27] The stresses change very little with different dynamics (they are due to elastic propagation of gravity forces), and the dissipation is essentially the inverse of the plate viscosity. In other words, stronger plates deform less and dissipate less energy [e.g., *Capitanio et al.*, 2007]. This leaves more energy for the other plate that can subduct more.

[28] In Figure 5 we can also note the size of the subduction channel, as the gap between the downgoing and overriding plate. The low viscosity overriding plate model evolves with a smaller channel than the high viscosity overriding plate model. As the slab going down beneath the high viscosity overriding plate moves faster the force exerted on the overriding plate not only extends the plate, but also pushes it further from the hinge. The initial gap (seen in Figure 1) is set and then subsequently minimized by the contact algorithm. However the contact algorithm utilized has no equivalent 'pulling' regime, so

the only force moving the overriding plate toward the trench is the basal tractions from the induced flows beneath. And thus, there is no intraplate stress propagation between the plates.

[29] Isosurface bulging evident in the models, also seen in Figure 5, is a proxy for the free-Earth surface expression of dynamic topography. Such dynamic topography is due exclusively to the viscous flow in the mantle. Imposing an overriding plate masks the topography as the flow energy interacts with the plate instead of moving the free-Earth surface. However, flexural bulging along the plate isosurfaces is evident due to the mass entering the mantle and the viscosity of the plate causing the plate to bend (bulge).

[30] We consider the plate velocity for each model as being the angular speed at the Euler pole for each timestep, of the unsubducted part of the subducting plate. Overriding plate angular speed is calculated similarly. Figure 6 shows the forward velocities of the subducting plates for each model at 10 m.y. and the corresponding overriding plate velocity. We define the direction of subducting plate advance as the positive Z-direction from Figure 1. This figure is typical of the relative speed of the subducting plate through time, however beyond about 17 m.y. all velocities enter an oscillatory stage, with higher viscosity models having longer wavelength features than lower viscosity models.

[31] Models with overriding plate viscosity of 10–150η_m show similar deformation styles and velocities up to 17 m.y. of evolution. In this time frame high-viscosity models tend to sink faster than low-viscosity models, resulting in deeper subduction with a steeper dip angle. Subducting plates will advance forward through time, with the amount of slab-rollback dependent on the properties of the overriding plate. High-viscosity models also show increased plate advance but with enough slab-rollback to maintain equivalent trench position with the low-viscosity models, this is indicated by the positions of the subducting plate's trailing edge and the trench. Still, we find the Slab-Only model show the most slab-rollback. We find that the trench velocity, V_t compared with the subducting plate velocity, V_{sp}, for the Slab-Only model is $\frac{V_t}{V_{sp}} = 1$, and the OP model shows $\frac{V_t}{V_{sp}} = 0.35$, averaged over the model run.

[32] The general pattern of strain on the overriding plate for the OP model (with $\eta_{op} = 50\eta_m$) shown in Figure 3 is consistent for the high and low-viscosity models but showing different magnitudes. Low-viscosity overriding plate models show minimal
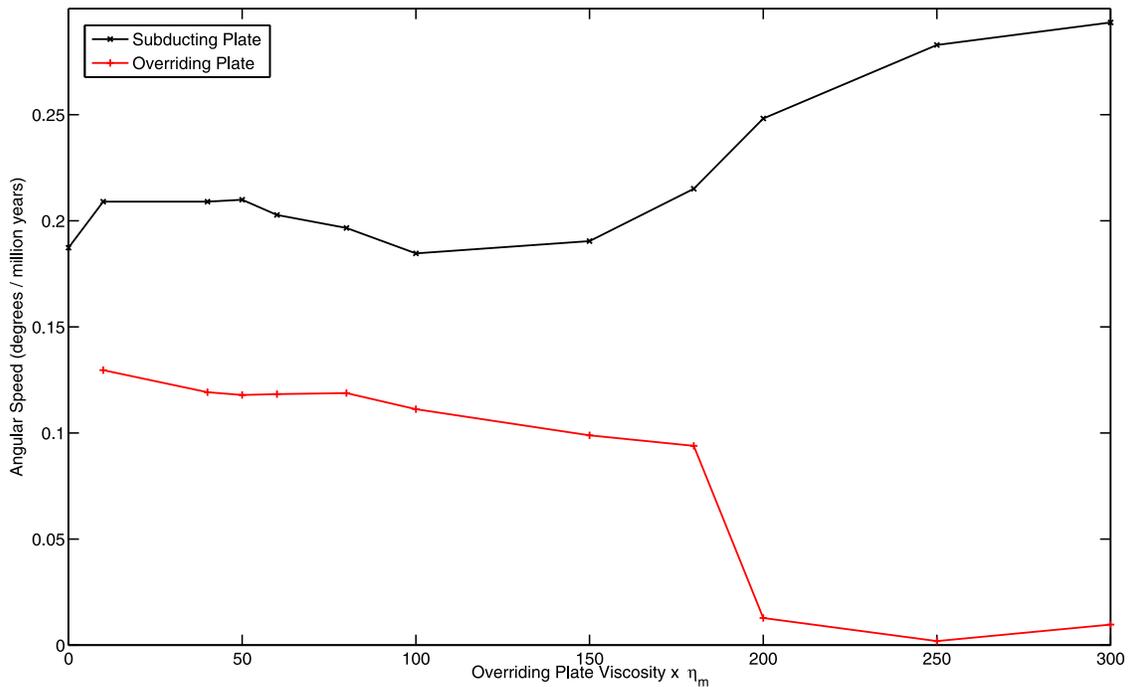
Figure 6. Angular speed of the subducting and overriding plates compared against different overriding plate viscosities at 10 m.y. The subducting and overriding plates are both moving toward the trench, thus the plate speeds are opposite in direction. Angular speed is determined from the plate's Euler pole and averaged every 10 timesteps. Models with $\eta_{op} > 180\eta_m$ have a faster moving subducting plate than models with $\eta_{op} < 180\eta_m$. The model with $\eta_{op} = 0\eta_m$ is the Slab-Only model, and does not have an overriding plate isosurface.

extensive deformation in the overriding plate, and overriding plates $<80\eta_m$ show compressive deformation. The magnitude of deformation increases as viscosity deviates from $\eta_{op} = 80\eta_m$. When the trench velocity approximately equals the overriding plate velocity the back-arc strain is not significant, consistent with the 'neutral line' from *Lallemand et al.* [2008]. High-viscosity models exhibit extension through all time. Low-viscosity overriding plate models and the Slab-Only model results in highest plane stress on the advancing face of the subducting slab either side of the trench, showing similar stress patterns to *van Dinther et al.* [2010]. High-viscosity overriding plate models display more deformation over the entire subducting plate compared to the low-viscosity models. For all models, the strain in the overriding plate becomes more pronounced during periods of subducting plate acceleration, e.g., between 15–19 m.y. During these periods, the entire subducting plate experiences increased deformation compared to lower acceleration periods.

[33] Here we have modeled a fixed geometry with varying overriding plate viscosity to try to gain an understanding of what relatively high and low overriding plate viscosities will have on the evolution of a down-going slab. In all models evolution reveals an upward bending in the forepart of the subducting slab, similar to the models by *Yamato et al.* [2009], even without a mantle viscosity discontinuity that other models generally have. High-viscosity overriding plates cause the subducting plate to evolve quicker than equivalent subducting plates with a low-viscosity overriding plate. The same conclusions are found when the two interacting plates are up to 2× wider, and when the down-going plate's viscosity is increased to $100 \times \eta_m$.

4. Thin-Sheet Analysis of Plate Driving Forces

[34] Each model is independently a good representation of natural subduction, however because of the time-dependency of the models, having implicitly defined time steps with an evolving slab geometry, direct comparison between models is not accurate. As such, we are motivated by the 2-D BEM analysis of *Ribe* [2010] to define geometric

and kinematically defined characteristic quantities which are consistent between models.

[35] We simplify our 3-D analysis by taking a trench-orthogonal row of panels along the upper surface of the subducting plate and project them onto the YZ-plane (removing minor X-direction perturbations). The angle between the unit normal of the panel, $\hat{n}$, and inclination unit vector $\hat{e}_\theta$ is thus related to the trench-ward dip of each panel, θ_D, by

$$\theta_D = \cos^{-1}(\hat{n} \cdot \hat{e}_\theta) - \frac{\pi}{2}. \qquad (1)$$

[36] Now to determine model-independent subducting plate properties, we use the definition of *Ribe* [2003, 2010] for curvature (K) defined along the plate's surface (s) as

$$K = -\frac{\partial \theta_D}{\partial s}. \qquad (2)$$

[37] This leads to the definition of a subducting plate's bending length, ℓ_b. We take ℓ_b as the distance from the tip of advancing face of the slab to the global minimum of K. We use these quantities to determine the forces acting in the models.

[38] The velocity of the down-going slab corresponds to the forces acting upon and within it. It has been shown previously by *Forsyth and Uyeda* [1975] and *Schellart* [2004] that the buoyancy force acting to pull the slab down into the mantle can be approximated by

$$F_b \sim T_s \ell_s W_s \Delta\rho_s g. \qquad (3)$$

[39] Also, the force acting in the forward limb of a subducting slab responsible of the resistance to bending (or slab straightening force) is given per unit length of the trench by [*Ribe*, 2001]

$$F_r \sim \eta_s V \left(\frac{T_s}{l_b}\right)^3. \qquad (4)$$

[40] Finally, there is a resistive viscous drag force on a slab moving in the surrounding mantle with a sinking velocity of V. As shown in *Happel and Brenner* [1983] and *Capitanio et al.* [2007, Appendix A], this force may be approximated by that over a thin ellipsoid with semi-axes $a > b \gg c$ which is given by

$$F_d \sim \frac{\eta_m V a}{1 + \log(a/b)} \qquad (5)$$

The drag force over the overriding plate is in turn proportional to its velocity U_{op} and area A

$$F_{dop} \sim \eta_m U_{op} A \qquad (6)$$

Now, the downward acting buoyant force incites a flow beneath and above the face of the down-going slab causing tractions between the plates. So, the relative velocity between the overriding plate and the down-going slab gives an indication to the relative contributions of the forces acting. Thus we may determine the distribution of forces in each of the models.

[41] Previous plate driving force analysis like that of *Conrad and Lithgow-Bertelloni* [2004] have a net torque within the models due to the imposed pulling force, they correct for this by summing the torques and subtracting the difference. In our BEM-Earth models we produce torque in an absolute frame where only gravity moves material self-consistently, so the total angular momentum of the system is preserved.

[42] We measure a plate's resistance to bending compared to drag in analogy with the definition of the 'stiffness' of a subducting plate given by *Ribe* [2010]

$$\frac{F_r}{F_d} \sim \frac{\eta_s}{\eta_m}\left(\frac{T_s}{\ell_b}\right)^3 \frac{W_s}{a}[1 + \log(a/b)] \equiv S. \qquad (7)$$

This is a measure of a plate's resistance to bending compared to drag along the trench-parallel extent of the subducting plate, W_s.

[43] Cases tested here represent $S < 1$, thus the trench rollback we see in Figure 2 is expected [*Di Giuseppe et al.*, 2008]. There is indication that larger (wider and longer) overriding plates will cause the down-going slab's ℓ_b to evolve slower compared to the smaller (narrower and shorter) overriding plates. By comparison, we find the change in S due to the overriding plate area is at most equivalent to doubling η_s. It is also found lower viscosity overriding plates couple to slabs resulting in high S and vice-versa. Further model runs show S is influenced by the width of the subducting plate. Wider subducting plates generally have increased drag with or without an overriding plate, so S increases.

[44] We can also consider the ratio of the overriding plate drag (F_{dop}) to the down-going slab bending resistance (F_r) representative of a suction type force acting through the poloidal flows coupling the

overriding plate and the down-going slab. We observe that longer models have a lower ratio compared to the shorter models. Generally we find this suction force greatest in the shorter models. We find in quasi-steady state periods the mean difference between $\frac{F_{dop}}{F_r}$ is most affected by the trench-orthogonal length of the overriding plate. Here the difference of $\frac{F_{dop}}{F_r}$ between longer and shorter overriding plate models of equivalent width is $\sim 4.2 \times 10^4$. The mean difference between models of different widths and equivalent length is $\sim 0.5\times$ smaller, suggesting overriding plate width is not as an important factor as length in coupling the plates.

[45] Finally, we consider the ratio of F_{dop} to slab drag (F_d). We find a similar distribution of forces as in the $\frac{F_{dop}}{F_r}$ relationship. Again, during periods of quasi-steady state there is a distinct force partitioning between the long and shorter models, with shorter models having a greater F_{dop}. We find that the mean difference of $\frac{F_{dop}}{F_d}$ between the longer and shorter overriding plate models of equivalent widths to be $\sim 1.4 \times 10^5$. The models can be further distinguished by the relative width of the overriding plates, so the narrow plate has the lowest and the wide plate the highest F_{dop} to F_d ratio. As such, $\frac{F_{dop}}{F_d}$ is found to be $\sim 0.5\times$ smaller when comparing models of different overriding plate widths of equivalent length.

[46] Geometric dimensions in the models influence the distribution of forces between the plates. Similar analysis shows high-viscosity overriding plates do not couple as strongly as low-viscosity overriding plates to the down-going slab. Because F_b will be consistent between models, as the amount of material is consistent in each model, we conclude that the different induced suction forces in each of the overriding plate models is causing the change in the plate motion.

5. Discussion and Conclusions

[47] The presence of an overriding plate along the subduction zone reduces the trench-orthogonal motion of the subducting plate directly beneath it, suggesting that poloidal flows dominate the coupling between the subducting slab and the overriding plate. This is backed up by the trench-parallel width of the overriding plate, compared with the trench-orthogonal length of the overriding plate, having a lesser effect on the suction forces coupling the down-going slab and overriding plate. These

results maintain that the presence of an overriding plate tends to slow trench migration [*Yamato et al.*, 2009; *Capitanio et al.*, 2010].

[48] The quantity S can be a good proxy for plate bending curvature [*Wu et al.*, 2008]. Our models suggest that the geometrical and rheological properties of the overriding plate contribute to the stiffness of the down-going plate through the flows coupling the plates together. We find that the strongest coupling of $\frac{F_{dop}}{F_d}$ and $\frac{F_{dop}}{F_r}$ between the subducting and overriding plates (seen in the OP-Wide model) leads to shortening in the overriding plate. As the width of the overriding plate is reduced (OP and OP-Narrow models) the coupling suction decreases and the overriding plate deformation moves into extension. This is compared with weaker coupling in longer (OP-Long/Wide, OP-Long, OP-Long/Narrow) overriding plates that show more extension in the back-arc region. *Capitanio et al.* [2011] and *Laffaldano et al.* [2012] considered shear force gradients and intraplate frictional forces respectively of the Nazca-South American plate system to help account for Andean topography. The deformation seen in Figures 2–4 suggests the area of the overriding plate mechanically coupled to the down-going plate influences the shear and intraplate forces that can result in the formation of Andean style topography.

[49] We identify two subduction regimes associated with different overriding plate viscosities: subducting slabs influenced by high-viscosity overriding plates ($\eta_{op} > 180\eta_m$) or by low-viscosity overriding plates ($\eta_{op} < 180\eta_m$). High-viscosity overriding plates increase subducting plate velocity and produce slabs with slightly more steeply dipping angles. The presence of the overriding plate changes the dynamics of the down-going plate, but also changing the viscosity of the overriding plate itself will affect the asthenospheric flow coupling the two plates together.

[50] Invariably our model setup predicates steep angle subduction like that seen in the Western-Pacific. Such deep angle subduction has been linked with back-arc basin formation [*Uyeda and Kanamori*, 1979; *Lallemand et al.*, 2005], subsequently we expect to see extension in the overriding plates in our models. Also, back-arc extension is expected to begin when the overriding plate moves away from trench [*Sdrolias and Müller*, 2006]. Overriding plates in our models generally move towards the trench as the slab rolls back. The length of the trench primarily used in this study is

comparable to back-arc systems encountered in nature. Also, the sizes of the overriding plates investigated are similar for the range of overriding plate sizes where back-arcs form. Whilst we find a clear connection in our models between overriding plate width, length and deformation, no such correlation seems to exist in nature. This is partially due to the lack of adjacent plates, that would change the natural movements of the plates. For low-viscosity models we find $V_{op} \approx V_t$, and coincidentally we find back-arc strain to be minimal [*Lallemand et al.*, 2008]. Further, the low-viscosity models show $V_{op} < 0$ and $V_{sp} > 0$. The correlation between deformation in these models to the back-arcs studied in *Lallemand et al.* [2008] is comparable.

[51] The change in subduction dynamics due to only the changing rheology suggests that a subducting plate may deform differently along the trench-parallel subduction extent as it subducts below an overriding plate with a heterogeneous rheology. This is exemplified by the Kamchatka subduction zone, north of Japan, where the subduction style changes along the subduction zone [*Li et al.*, 2008]. Towards the north the Pacific plate is moving relatively slowly at a steep angle, with the overriding plate in extension. Moving to the south, the overriding plate becomes more compressed, the Pacific plate increases speed and the dip angle shallows.

[52] Changing the thickness of the overriding plate has no clear affect on subducting plate dynamics, but influences the deformation in the overriding plate itself. This is consistent with *Capitanio et al.* [2010], but a recent study by *Rodríguez-González et al.* [2012] suggest that a varying trench-perpendicular overriding plate thickness can change subducting plate motion and style. The modeling technique used by *Rodríguez-González et al.* [2012] imposed plate kinematics and restricted vertical movements that may impact the results. Other non-subducting plates immediately behind, and lateral to, a subducting plate are found to slow subduction velocity and change the slab dip. Therefore non-subducting plates adjacent to subduction zones must be considered in more realistic models.

[53] The dynamic evolution of a subducting slab in a spherical setup is influenced by a variety of both intrinsic and external parameters. Inclusion of an overriding plate and other non-subducting plates changes the dynamics of a subduction system by altering velocities over the slab. The rheological and geometric properties of these plates change the

induced mantle flows coupling them with the down-going slab. This in-turn changes trench migrations and trench curvature. However, the attributes of the overriding plate studied here generate secondary effects that are overwhelmed by other forcings on the system [*Schellart*, 2004; *Capitanio et al.*, 2010; *van Dinther et al.*, 2010]. It appears the down-going slab is the main driver for overriding plate dynamics, in terms of rheology and stress [*Billen*, 2008; *Capitanio et al.*, 2011].

[54] BEM-Earth is emerging as an intermediately complex subduction model framework [*Gerya*, 2011], with simple environmental set-ups with realistic physical model drivers. Dynamically driven models produced in BEM-Earth can provide insights into subduction systems, by easily isolating individual parameters for testing. The nature of the models allows for further complications to be added approaching more complex realistic scenarios at the global scale [*Morra et al.*, 2012].

Appendix A

A1. Contact Parameter Affect

[55] The isosurface separation parameter, h, and the isosurface interaction distance, control the interactions between the isosurfaces. These contact parameters are empirically determined, with the order of $h \sim T_s$, at the beginning of each suite of experiments and kept constant across simulations to be compared. If the contact layer, h, is too small instabilities arise during the computation. If h is too large the uplifting force is not properly calculated so the plate isosurface in 'contact' with the external isosurface will detach and sink vertically into the mantle. This is a standard numerical modeling practice [*Morra et al.*, 2007; *OzBench et al.*, 2008; *Schmeling et al.*, 2008; *Ribe*, 2010] and its implementation in BEM-Earth is detailed in *Morra et al.* [2012, Appendix D].

[56] Different model dynamics can be due to the strength of the contact parameter or due to the altered flow from the presence of an overriding plate. We consider the trench dynamics for determining these relative effects. We analyze 3 sets of well-evolved (22 m.y.) models by changing the contact parameter between the upper ($h = T_s \times 0.42$) and lower stability ($h = T_s \times 0.38$) bounds for these models. We then compare the results to the contact parameter used in the analysis ($h = T_s \times 0.4$). We find the maximum change in the amount

of trench-rollback from the initial position is; 26% increased rollback for the OP models; 8% for the OP-Narrow models; and 15% for the Slab-Only models. Trench morphology is also influenced by the contact. Again, changing the contact within the stability bounds results in at-most a median deviation (from the curvature of the model with the stable contact) of; 1% for the OP models; 2% for the OP-Narrow models; and 5% for the Slab-Only models. Thus, we find flow changes due to the presence of an overriding plate overwhelm the effect of the contact when considering trench morphology and trench-rollback, when the contact parameters are held constant between simulations.

A2. Ridge Push Affect

[57] We use two models, OP and OP with 5% of the trailing edge chamfered. We contrast the bending length of each model at each timestep up to 268 ($\sim$17 m.y.), the time that the chamfered model breaks down by crossing the free-surface. We measure the absolute deviation as $\frac{\ell_{bop} - \ell_{bsharpen}}{\ell_{bop}}$, and find this to be at most 4.792% with a median of 0.003% and a mean of 0.080%. The small amount of deviation allows us to remove this feature from the models.

A3. Thin Sheet Derivation

[58] We take a YZ-plane strip of panels and then transform each panel's coordinates into a spherical coordinate system, and determine a basis unit vector for each panel. Using the centroid of the panel given by position vector, $\vec{r} = (x, y, z)$ in spherical coordinates as $\vec{r} = (\rho, \theta, \phi)$ where

$$\begin{pmatrix} \rho \\ \theta \\ \phi \end{pmatrix} = \begin{pmatrix} \sqrt{x^2 + y^2 + z^2} \\ \cos^{-1}\frac{z}{\rho} \\ \tan^{-1}\frac{y}{x} \end{pmatrix}.$$

[59] And the basis unit vectors are determined as

$$\begin{pmatrix} \hat{e}_\rho \\ \hat{e}_\theta \\ \hat{e}_\phi \end{pmatrix} = \begin{pmatrix} \sin\theta\cos\phi, \sin\theta\sin\phi, \cos\theta \\ \cos\theta\cos\phi, \cos\theta\sin\phi, -\sin\theta \\ -\sin\phi, \cos\phi, 0 \end{pmatrix}.$$

[60] The angle between the unit normal of the panel, $\hat{n}$, and inclination unit vector $\hat{e}_\theta$ is thus related to the trench-ward dip of each panel, θ_D, by

$$\theta_D = \cos^{-1}(\hat{n} \cdot \hat{e}_\theta) - \frac{\pi}{2}. \tag{A1}$$

[61] We also use the orthogonal or normal velocity of the panel, $W = \hat{n} \cdot \vec{v}$, and the longitudinal or

tangential velocity, $U = \vec{d} \cdot \vec{v}$, where $\vec{v}(x, y, z)$ is the velocity of the panel, and $\vec{d}(x, y, z)$ is the displacement vector between two adjacent panel centroids.

[62] Now to determine model-independent slab properties, we use the definitions of *Ribe* [2003, 2010] for curvature (K), stretching (Δ), rotation (ω), and curling ($\dot{K}$):

$$K = -\frac{\partial \theta_D}{\partial s} \tag{A2}$$

$$\Delta = \frac{\partial U}{\partial s} - KW \tag{A3}$$

$$\omega = \frac{\partial W}{\partial s} + KU \tag{A4}$$

$$\dot{K} = \frac{\partial \omega}{\partial s} - K\Delta. \tag{A5}$$

[63] Numerical differentiation along the slab surface, s, is computed using a smooth noise-robust method (P. Holoborodko, Smooth noise robust differentiators, http://www.holoborodko.com/pavel/numerical-methods/numerical-derivative/smooth-low-noise-differentiators/, 2008) such that the derivative of any function, f, is given by

$$f' = \frac{2(f_{s_1} - f_{s_{-1}}) + f_{s_2} - f_{s_{-2}}}{2(s_2 - s_{-2})} \tag{A6}$$

with f' of the first and last 2 panels initialized to 0.

Acknowledgments

References

Arcay, D., S. Lallemand, and M. P. Doin (2008), Back-arc strain in subduction zones: Statistical observations versus

numerical modeling, *Geochem. Geophys. Geosyst.*, *9*, Q05015, doi:10.1029/2007GC001875.

Becker, T. W., and C. Faccenna (2009), A review of the role of subduction dynamics for regional and global plate motions, in *Subduction Zone Geodynamics*, edited by S. Lallemand and F. Funiciello, pp. 3–34, Springer, Berlin, doi:10.1007/978-3-540-87974-9_1.

Becker, T. W., and R. J. O'Connell (2001), Predicting plate velocities with mantle circulation models, *Geochem. Geophys. Geosyst.*, *2*(12), 1060, doi:10.1029/2001GC000171.

Bellahsen, N. (2005), Dynamics of subduction and plate motion in laboratory experiments: Insights into the "plate tectonics" behavior of the earth, *J. Geophys. Res.*, *110*, B01401, doi:10.1029/2004JB002999.

Billen, M. I. (2008), Modeling the dynamics of subducting slabs, *Annu. Rev. Earth Planet. Sci.*, *36*, 325–356, doi:10.1146/annurev.earth.36.031207.124129.

Capitanio, F. A., G. Morra, and S. Goes (2007), Dynamic models of downgoing plate-buoyancy driven subduction: Subduction motions and energy dissipation, *Earth Planet. Sci. Lett.*, *262*, 284–297, doi:10.1016/j.epsl.2007.07.039.

Capitanio, F. A., G. Morra, and S. Goes (2009), Dynamics of plate bending at the trench and slab-plate coupling, *Geochem. Geophys. Geosyst.*, *10*, Q04002, doi:10.1029/2008GC002348.

Capitanio, F. A., D. R. Stegman, L. N. Moresi, and W. Sharples (2010), Upper plate controls on deep subduction, trench migrations and deformations at convergent margins, *Tectonophysics*, *483*, 80–92, doi:10.1016/j.tecto.2009.08.020.

Capitanio, F. A., C. Faccenna, S. Zlotnik, and D. R. Stegman (2011), Subduction dynamics and the origin of Andean orogeny and the Bolivian orocline, *Nature*, *480*, 83–86, doi:10.1038/nature10596.

Clark, S. R., D. R. Stegman, and R. D. Müller (2008), Episodicity in back-arc tectonic regimes, *Phys. Earth Planet. Inter.*, *171*, 265–279, doi:10.1016/j.pepi.2008.04.012.

Conrad, C. P., and C. Lithgow-Bertelloni (2004), The temporal evolution of plate driving forces: Importance of slab suction versus slab pull during the Cenozoic, *J. Geophys. Res.*, *109*, B10407, doi:10.1029/2004JB002991.

Di Giuseppe, E., J. van Hunen, F. Funiciello, C. Faccenna, and D. Giardini (2008), Slab stiffness control of trench motion: Insights from numerical models, *Geochem. Geophys. Geosyst.*, *9*, Q02014, doi:10.1029/2007GC001776.

Forsyth, D., and S. Uyeda (1975), On the relative importance of the driving forces of plate motion, *Geophys. J. R. Astron. Soc.*, *43*, 163–200.

Funiciello, F., G. Morra, K. Regenauer-Lieb, and D. Giardini (2003), Dynamics of retreating slabs: 1. Insights from two-dimensional numerical experiments, *J. Geophys. Res.*, *108*(B4), 2206, doi:10.1029/2001JB000898.

Funiciello, F., C. Faccenna, and D. Giardini (2004), Role of lateral mantle flow in the evolution of subduction systems: insights from laboratory experiments, *Geophys. J. Int.*, *157*, 1393–1406, doi:10.1111/j.1365-246X.2004.02313.x.

Gerya, T. (2011), Future directions in subduction modeling, *J. Geodyn.*, *52*(5), 344–378, doi:10.1016/j.jog.2011.06.005.

Happel, J., and H. Brenner (1983), *Low Reynolds Number Hydrodynamics: With Special Applications to Particulate Media*, Martinus Nijhoff, The Hague, Netherlands.

Laffaldano, G., E. Di Giuseppe, F. Corbi, F. Funiciello, C. Faccenna, and H.-P. Bunge (2012), Varying mechanical coupling along the Andean margin: Implications for trench curvature, shortening and topography, *Tectonophysics*, *526–529*, 16–23, doi:10.1016/j.tecto.2011.09.014.

Lallemand, S., A. Heuret, and D. Boutelier (2005), On the relationships between slab dip, back-arc stress, upper plate absolute motion, and crustal nature in subduction zones, *Geochem. Geophys. Geosyst.*, *6*, Q09006, doi:10.1029/2005GC000917.

Lallemand, S., A. Heuret, C. Faccenna, and F. Funiciello (2008), Subduction dynamics as revealed by trench migration, *Tectonics*, *27*, TC3014, doi:10.1029/2007TC002212.

Li, C., R. D. van der Hilst, E. R. Engdahl, and S. Burdick (2008), A new global model for P wave speed variations in Earth's mantle, *Geochem. Geophys. Geosyst.*, *9*, Q05018, doi:10.1029/2007GC001806.

Mahadevan, L., R. Bendick, and H. Liang (2010), Why subduction zones are curved, *Tectonics*, *29*, TC6002, doi:10.1029/2010TC002720.

Morra, G., K. Regenauer-Lieb, and D. Giardini (2006), Curvature of oceanic arcs, *Geology*, *34*(10), 877–880, doi:10.1130/G22462.1.

Morra, G., P. Chatelain, P. Tackley, and P. Koumoutsakos (2007), Large scale three-dimensional boundary element simulation of subduction, in *Computational Science–ICCS 2007, Part III*, *Lect. Notes Comp. Sci.*, vol. 4489, pp. 1122–1129, Springer, Berlin.

Morra, G., P. Chatelain, P. Tackley, and P. Koumoutsakos (2009), Earth curvature effects on subduction morphology: Modeling subduction in a spherical setting, *Acta Geotechnica*, *4*, 95–105, doi:10.1007/s11440-008-0060-5.

Morra, G., L. Quevedo, and R. D. Müller (2012), Spherical dynamic models of top-down tectonics, *Geochem. Geophys. Geosyst.*, *13*, Q03005, doi:10.1029/2011GC003843.

OzBench, M., et al. (2008), A model comparison study of large-scale mantle–lithosphere dynamics driven by subduction, *Phys. Earth Planet. Inter.*, *171*(1–4), 224–234, doi:10.1016/j.pepi.2008.08.011.

Pozrikidis, C. (1992), *Boundary Integral and Singularity Methods for Linearized Viscous Flow*, Cambridge Univ. Press, Cambridge, U. K.

Ribe, N. M. (2001), Bending and stretching of thin viscous sheets, *J. Fluid. Mech.*, *433*, 135–160.

Ribe, N. M. (2003), Periodic folding of viscous sheets, *Phys. Rev. E*, *68*, 036305, doi:10.1103/PhysRevE.68.036305.

Ribe, N. M. (2010), Bending mechanics and mode selection in free subduction: A thin-sheet analysis, *Geophys. J. Int.*, *180*, 559–576, doi:10.1111/j.1365-246X.2009.04460.x.

Rodríguez-González, J., A. M. Negredo, and M. I. Billen (2012), The role of the overriding plate thermal state on slab dip variability and on the occurrence of flat subduction, *Geochem. Geophys. Geosyst.*, *13*, Q01002, doi:10.1029/2011GC003859.

Schellart, W. P. (2004), Quantifying the net slab pull force as a driving mechanism for plate tectonics, *Geophys. Res. Lett.*, *31*, L07611, doi:10.1029/2004GL019528.

Schellart, W. P. (2005), Influence of the subducting plate velocity on the geometry of the slab and migration of the subduction hinge, *Earth Planet. Sci. Lett.*, *231*, 197–219, doi:10.1016/j.epsl.2004.12.019.

Schellart, W. P. (2008a), Subduction zone trench migration: Slab driven or overriding-plate-driven?, *Phys. Earth Planet. Inter.*, *170*, 73–88, doi:10.1016/j.pepi.2008.07.040.

Schellart, W. P. (2008b), Kinematics and flow patterns in deep mantle and upper mantle subduction models: Influence of the mantle depth and slab to mantle viscosity ratio, *Geochem. Geophys. Geosyst.*, *9*, Q03014, doi:10.1029/2007GC001656.

Schellart, W. P., J. Freeman, D. R. Stegman, L. Moresi, and D. May (2007), Evolution and diversity of subduction zones

controlled by slab width, *Nature*, *446*, 308–311, doi:10.1038/nature05615.

Schellart, W. P., D. R. Stegman, R. Farrington, J. Freeman, and L. Moresi (2010), Cenozoic tectonics of western North America controlled by evolving width of farallon slab, *Science*, *329*, 316–319, doi:10.1126/science.1190366.

Schmeling, H., et al. (2008), A benchmark comparison of spontaneous subduction models–Towards a free surface, *Phys. Earth Planet. Inter.*, *171*, 198–223, doi:10.1016/j.pepi.2008.06.028.

Sdrolias, M., and R. D. Müller (2006), Controls on back-arc basin formation, *Geochem. Geophys. Geosyst.*, *7*, Q04016, doi:10.1029/2005GC001090.

Stegman, D. R., J. Freeman, W. P. Schellart, L. Moresi, and D. May (2006), Influence of trench width on subduction hinge retreat rates in 3-D models of slab rollback, *Geochem. Geophys. Geosyst.*, *7*, Q03012, doi:10.1029/2005GC001056.

Stegman, D. R., R. Farrington, F. A. Capitanio, and W. P. Schellart (2010a), A regime diagram for subduction styles from 3-d numerical models of free subduction, *Tectonophysics*, *483*, 29–45, doi:10.1016/j.tecto.2009.08.041.

Stegman, D. R., W. P. Schellart, and J. Freeman (2010b), Competing influences of plate width and far-field boundary conditions on trench migration and morphology of subducted slabs in the upper mantle, *Tectonophysics*, *483*, 46–57, doi:10.1016/j.tecto.2009.08.026.

Uyeda, S., and H. Kanamori (1979), Back-arc opening and the mode of subduction, *J. Geophys. Res.*, *84*(B3), 1049–1061, doi:10.1029/JB084iB03p01049.

van Dinther, Y., G. Morra, F. Funiciello, and C. Faccenna (2010), Role of the overriding plate in the subduction process: Insights from numerical models, *Tectonophysics*, *484*, 74–86, doi:10.1016/j.tecto.2009.08.038.

Wu, B., C. P. Conrad, A. Heuret, C. Lithgow-Bertelloni, and S. Lallemand (2008), Influence of the subducting plate velocity on the geometry of the slab and migration of the subduction hinge, *Earth Planet. Sci. Lett.*, *272*, 412–421, doi:10.1016/j.epsl.2008.05.009.

Yamato, P., L. Husson, J. Braun, C. Loiselet, and C. Thieulot (2009), Influence of surrounding plates on 3D subduction dynamics, *Geophys. Res. Lett.*, *36*, L07303, doi:10.1029/2008GL036942.

Zhong, S. (2001), Role of ocean-continent contrast and continental keels on plate motion, net rotation of lithosphere, and the geoid, *J. Geophys. Res.*, *106*(B1), 703–712.